We are IntechOpen, the world's leading publisher of Open Access books Built by scientists, for scientists

4,800
Open access books available

122,000
International authors and editors

135M
Downloads

Our authors are among the

154
Countries delivered to

TOP 1%
most cited scientists

12.2%
Contributors from top 500 universities

CLARIVATE ANALYTICS BOOK CITATION INDEX INDEXED

WEB OF SCIENCE™

Selection of our books indexed in the Book Citation Index in Web of Science™ Core Collection (BKCI)

Interested in publishing with us?
Contact book.department@intechopen.com

Numbers displayed above are based on latest data collected.
For more information visit www.intechopen.com

1

Nematic Liquid Crystal Confined in Electrochemically Etched Porous Silicon: Optical Characterization and Applications in Photonics

Georgiy V. Tkachenko[1], Volodymyr Tkachenko[2], Giancarlo Abbate[2], Luca De Stefano[3], Ilaria Rea[3] and Igor A. Sukhoivanov[4]
[1]*Kharkov National University of Radio Electronics,*
[2]*CNR-INFM Lab Coherentia, Università di Napoli Federico II,*
[3]*Istituto per la Microelettronica e Microsistemi (CNR-IMM),*
[4]*Universidad de Guanajuato,*
[1]*Ukraine*
[2,3]*Italy*
[4]*Mexico*

1. Introduction

Liquid crystals (LC) confined in curved geometries have been a fundamental challenge for more than a century, starting from the study of supra-micrometre nematic droplets suspended in an isotropic medium (Lehmann, 1904). In the mid-1980s, a new period began with this topic stimulated by the discovery of various composite materials suitable for electro-optic and thermo-optic applications in controllable light scattering windows, flat-panel displays, holography, optical networking, and computing. In these materials LC molecules are confined within polymer or porous networks, therefore a competition arises between surface ordering and disordering effects on formation of stable director configurations and configurational transitions, critical temperatures of mesogenic phase transitions, orientational and hydro-dynamics and other properties. So far the behaviour of mesogens enclosed in different porous matrixes such as Nuclepore polymer membrane, Anopore aluminium oxide membrane, Vycor glass, and others with pores of different size and shape have been investigated by means of various experimental techniques: specific heat calorimetry, nuclear magnetic resonance, dielectric spectroscopy, polarization microscopy, dynamic light scattering etc.; for a review see (Crawford & Žumer, 1996).
Another host material namely electrochemically etched porous silicon (PSi) (Canham, 1997) has appeared to be promising for tunable and switchable optoelectronic devices due to the simplicity of fabrication, flexibility in wavelength design and compatibility with silicon microelectronic technology. Since PSi film is only several microns thick, most of the above mentioned techniques exhibit difficulties in its characterisation. Analysis of PSi-LC composite is complicated by the anisotropic nature of both the PSi matrix and the infiltrated LC. Nevertheless, an advanced technique developed for characterization of thin films,

Source: New Developments in Liquid Crystals, Book edited by: Georgiy V. Tkachenko,
ISBN 978-953-307-015-5, pp. 234, November 2009, I-Tech, Vienna, Austria

namely variable angle spectroscopic ellipsometry, can give crucial information on the amount of the infiltrated LC and preferential director orientation inside the pores (Marino et al., 2007).
The great advantage of PSi technology is an opportunity to fabricate multilayer structures with customized porosity and thickness of each layer. These structures are used in photonic devices such as Bragg reflectors (Pavesi & Dubos, 1997), optical microcavities (Weiss & Fauchet, 2003; Ouyang et al., 2005; Weiss et al., 2005; De Stefano et al., 2007), and even nonperiodic sequences, such as quasi-crystals (Moretti et al., 2006). Despite the many experimental and theoretical studies of the PSi-based 1-D photonic bandgap structures, rigorous simulations of their tuning properties, when filled with LC, have been scarce. Actually two rough approximations were usually done: first, the pores were considered filled with LC completely; second, the spatial distribution of the LC director was not taken into account or the simplest uniform axial configuration (the director oriented along the pore axis) was assumed. Whereas more complicated director configuration in the Si macropores with a diameter more than 1 micron were observed (Leonard et al., 2000; Haurylau et al., 2006], for the pores with a diameter less than 150 nm there is a lack of experimental information on the nematic director configuration.
Both electrical and thermal tuning has been achieved in the PSi-LC photonic bandgap microcavity realized on a silicon wafer (Weiss et al., 2005). Applying an electric field along the pore channels, the electrical reorientation of the LC with positive dielectric anisotropy was obtained. This fact indicates the non-axial orientation of the LC director inside the pores without field. However, more detailed study of the orientational properties of LC molecules in pores and their influence on the PSi-LC microcavity spectrum is still needed.
In the present chapter we are focusing on properties of a nematic LC confined in porous silicon with random pore distribution to be used in 1-D photonic devices. Section 2 gives a brief excursus into the physics of porous silicon and describes the methods applied for fabrication of monolayer, multilayer and free-standing PSi films; techniques for oxidation of the samples and infiltration with liquid crystals are also described. In the Section 3 we present the results of an ellipsometric study of refractive indices and birefringence of PSi and porous silica ($PSiO_2$) monolayers infiltrated with the commonly used nematic liquid crystal mixture E7. The effective ordinary and extraordinary refractive indices of the confined LC are derived from the experimental data using the effective medium approximation (EMA) model for the anisotropic composite. The temperature dependence of the refractive indices is compared with that in a bulk. Section 4 is dedicated to theoretical and experimental study of a free-standing PSi microcavity placed in a glass cell and infiltrated with E7. We present temperature dependence of the microcavity spectral characteristics and rigorous simulation of the LC effect on the spectral tuning. The distribution of the LC director within pores is simulated using the Frank's free energy approach. From the comparison between experimental spectra and the results of numerical calculations, we obtain the LC volume fraction in the composite, information on the LC director configuration inside the pores, and a rough estimate of the anchoring strength of LC molecules at the pore walls. In Section 5 we analyze the effect of an electric field on the director configuration of LC confined in pores and the PSi-LC microcavity spectrum.

2. Sample preparation and infiltration with liquid crystals

Porous silicon was discovered in the fifties trying to electropolish silicon in hydrofluoric acid (Uhlir, 1956, Turner, 1958). For low current densities, respectively high electrolyte

concentrations, silicon is not electropolished but pores are formed. Increasing the current density over a threshold value which decreases with the electrolyte concentration, results in electropolishing. In the beginning of the nineties visible luminescence in PSi at room temperature was discovered (Canham, 1990; Lehmann & Gösele, 1991). The possibility to produce optoelectronic devices based on PSi started enormous research activity. Meanwhile many applications for porous silicon are still developing. Most of these applications are based on the morphology of PSi.

PSi is formed by electrochemical etch of crystalline silicon wafers in HF-based solutions (Canham, 1997). The wafer is the anode; it is placed in back-side contact on an aluminum plate while the front side is sealed with an O-ring and exposed to the anodizing electrolyte. The cathode is made of platinum or any HF-resistant and conductive material. When a potential is applied to silicon in an aqueous environment, an electric current is induced to flow through the system.

The only important charge transfer reaction in the silicon/HF system is the reduction of water with the subsequent liberation of hydrogen gas. It is only under anodic polarizations that silicon dissolution occurs. The exact dissolution chemistries of silicon are still under debate, although it is generally accepted that holes h^+ are required in the initial steps for both electropolishing and pore formation. The dissolution mechanism can be expressed in the simplified reaction:

$$\mathrm{Si} + 6\mathrm{F}^- + 2\mathrm{H}^+ + 2\mathrm{h}^+ \rightarrow \mathrm{SiF}_6^{2-} + \mathrm{H}_2 \uparrow . \quad (1)$$

Heating and illumination increase the hole/electron pair generation in the substrate and affect the dissolution process. *P*-type silicon has an excess of holes, so it can be etched in a dark, whereas in the case of *n*-type silicon holes are minority carriers and illumination is generally required.

Due to quantum restrictions in thin Si walls, the electrochemical dissolution occurs only at the pore tips (Lehmann & Gösele, 1991). Thus pores are growing deep into the substrate according to the orientation of its crystal planes. Electrochemical etch of commonly used Si wafers with <100> orientation leads to the formation of columnar pores oriented normally to the plane of the silicon substrate (Canham, 1997).

PSi shows a great variety of morphologies dependent on the doping type and level in the silicon substrate and the electrochemical etching parameters. Usually for a given substrate and electrolyte, only one type of porous structure can be obtained. Guidelines of the International Union of Pure and Applied Chemistry define the ranges of pore sizes (Canham, 1997): pores characterized by a diameter less than 2 nm define microporous silicon; for sizes in the range 2-50 nm the PSi is mesoporous; pores having diameters more than 50 nm are typical for macroporous silicon. Highly doped *p*- or *n*-type silicon anodized in aqueous HF solution usually forms mesopores with sizes from 20 nm to 50 nm. In the case of lightly doped *p*-type silicon, the pore size distribution is normally found in the range 1 – 5 nm. The electrochemical etching of *n*-type substrates in the dark (for light doping) or with back-side illumination (for moderate doping) results in the formation of a macroporous material with radii in the micrometer range (Leonard et al., 1999).

The most important parameter of the PSi is the porosity, defined as the fraction of void within the porous layer. The porosity depends directly on the anodisation conditions and can be measured by means of gravimetric, profilometric or ellipsometric analysis of PSi

monolayers. We have used here the ellipsometric technique, which is discussed in the next section.

In the present work porous structures were fabricated using highly doped p+-silicon wafers with 0.01 Ω/cm resistivity and 400 μm thickness. The anodisation was performed in the HF-based solution (50 wt% HF : ethanol = 3:7) in the dark at room temperature. Electrochemical etch is quasi linear only for a short period of time (Canham, 1997), thus the pulses of electrical current were applied with duration of 0.2 s alternated with pauses of 5 s. The PSi structures formed in above-listed conditions were studied by means of the scanning electron microscope with a field emission gun (SEM-FEG Gemini 300, Carl Zeiss). As may be seen in Fig. 1 (a), the pores etched have average diameter of 50 nm, which corresponds to the threshold value between mesopores and macropores. Such pores are suitable for tunable PSi-based devices for near-infrared wavelength range: the pore size is large enough for infiltrating with different soft materials and at the same time it is much smaller than the wavelength, so scattering can be neglected and EMA can be used for electrodynamics simulation.

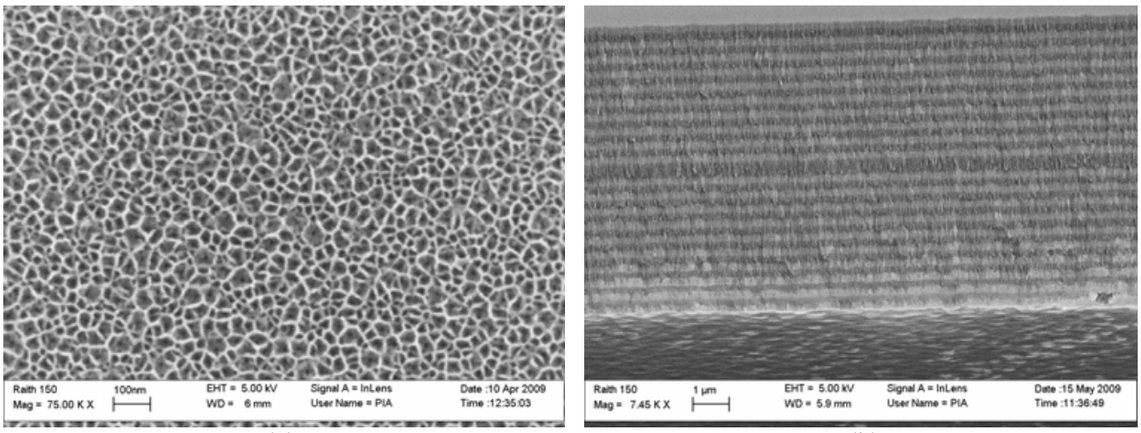

(a) (b)

Fig. 1. SEM-FEG image of a multilayer PSi: a) top-view, b) lateral view

For the given substrate, electrolyte and environment conditions (temperature and illumination), the porosity and etch rate are uniquely defined by the current density applied during the anodisation process (Canham, 1997). Thickness of the porous layer depends on the duration of the etch process monotonically. By changing the current applied and the duration of the etching it is possible to fabricate the multilayer PSi structures with desired porosity and thickness of each layer. Lateral view SEM-FEG image of a multilayer PSI is shown in Fig 1(b). It represents a couple of periodical structures with alternating layers of high and low porosity.

The multilayer PSi samples studied in this work were made free-standing by means of the Turner "lift-off" technique (Turner, 1958): at the end of etch process the current density was ramped to 800 mA/cm^2. That current density corresponds to the electropolishing mode and results in the PSi film detachment from the substrate. Free-standing films are thin and extremely fragile (Ghulinyan et al., 2003), however, this disadvantage is eliminated as soon as the film is placed inside a solid glass cell. But then the free-standing PSi film has some advantages as compared with the one on a wafer. A cell containing the PSi film can be filled with LC easily by the capillarity effect. Pores pass through the entire PSi film and are open

from both ends, so very high volume fractions of LC inside pores can be obtained. Furthermore, free-standing PSi-based optical devices can operate both in transmission and reflection modes, while on-wafer designs work only in reflection.

Fresh PSi is characterized by a high chemical reactivity. If stored in ambient air, the texture becomes partially oxidized, which leads to the change of its optical properties. To eliminate the problem of aging, the thermal oxidation of the structure is used. Usually, this treatment is also applied to PSi-based devices to utilize the visible range (Pirasteh et al., 2006). The oxidation reduces or completely removes silicon from the skeleton substituting it with SiO_2, which grows isotropically also into the pores. According to (Pirasteh et al., 2006), volume fraction of SiO_2 grown into silicon walls is twice as much as that grown into the void. PSi is generally oxidized in a pure O_2 atmosphere by a two step thermal treatment. The first oxidation step, defined as pre-oxidation, at low temperature (300 - 400 °C) is required in order to selectively oxidize the silicon backbonds thus assuring an easy propagation of the oxidant into the silicon structure. Moreover, the pre-oxidation reduces the damage of the material texture in the second oxidation step at higher temperatures between 800 and 900 °C (Pap et al., 2005).

Infiltration of the PSi and $PSiO_2$ samples with liquid crystal mixture E7 is performed under vacuum at the temperature above the clearing point of LC. The sample and LC are placed on the processor-controlled heater within a special vacuum chamber. The temperature is increased to 80°C and the chamber is evacuated to the pressure of about 1 Torr. At these conditions air and moisture are removed from the pores and liquid crystal. Then sample surface is completely covered by the LC drop. Liquid crystal fills the pores through capillary forces, low viscosity in isotropic phase facilitates infiltration. After about 5 hours, the pressure is rised to the atmospheric value, which pushes LC into the pores, providing excellent infiltration. After that the temperature is decreased slowly below the clearing point to promote LC transition to the nematic phase with equilibrium configuration of director.

3. Ellipsometric study of liquid crystals confined in porous Si and SiO_2

Standard spectroscopic ellipsometry is based on the measurement of two physical quantities: the relative amplitude change, Ψ, and the relative phase change, Δ, suffered by incident light when reflected (or transmitted) by a layered structure. These two parameters are linked to the reflection (or transmission) coefficients, which are themselves related to the optical response of the surface: the Ψ's and Δ's spectra depend on the refractive indices of the layers, on their thickness and, in the case of anisotropic films, on the orientation of their optical axis (of course, they depend on any physical parameters that affect the optical behaviour of the material, for instance on temperature).

For anisotropic media, generalised spectroscopic ellipsometry (GSE) is applied requiring the adoption of the 2×2 Jones matrix formalism. In this way it is possible to generalise the Ψ and Δ parameters to the case when a change occurs in the light polarisation. The six GSE parameters are linked to the Jones matrices of reflected ($\mathbf{J}^r$) or transmitted ($\mathbf{J}^t$) beam through the following equations:

$$\tan\Psi \cdot e^{i\Delta} = \frac{J_{pp}}{J_{ss}}; \quad \tan\Psi_{sp} \cdot e^{i\Delta_{sp}} = \frac{J_{sp}}{J_{ss}}; \quad \tan\Psi_{ps} \cdot e^{i\Delta_{ps}} = \frac{J_{ps}}{J_{pp}} \tag{2}$$

where $\mathbf{J} = \mathbf{J}^{\mathbf{r}}, \mathbf{J}^{\mathbf{t}}$; $\mathbf{J}^{\mathbf{r}} = \begin{pmatrix} r_{pp} & r_{sp} \\ r_{ps} & r_{ss} \end{pmatrix}$; $\mathbf{J}^{\mathbf{t}} = \begin{pmatrix} t_{pp} & t_{sp} \\ t_{ps} & t_{ss} \end{pmatrix}$ with r_{pp}, r_{ss}, r_{ps}, r_{sp} (t_{pp}, t_{ss}, t_{ps}, t_{sp}) representing the reflection (transmission) coefficients for *p*-, *s*-, and cross-polarisations, respectively.

Obtaining quantitative information on the wanted parameters of a sample requires setting of an optical model of the latter and a fit procedure matching the data generated by that model with the experimental ones. The mean squared error value, which is a measure of the difference between experimental and model data, is the indicator of the goodness of the employed model, as usual in GSE measurements.

Due to inherent inhomogeneity at mesoscale in the layer plane of porous silicon, the optical model is widely applied adopting the Bruggeman Effective Medium Approximation (EMA) (Spanier & Herman, 2000). As an electrochemically etched PSi contains anisotropically aligned nanowires and pores, the isotropic EMA has to be extended to take into account a form birefringence.

The pore shape effect can be examined by using adjustable depolarization factors L_i for ellipsoidal voids (*i* denotes projections along the main ellipsoid axes). For a <100> oriented Si wafer the depolarization factors fulfill the relations: $L_x=L_y=L_{xy}$ and $L_z+2L_{xy}=1$ (z axis is along the normal to the wafer). The components ε_i of the effective dielectric permittivity tensor of the PSi film are calculated using the generalized Bruggeman formula for two media (Spanier & Herman, 2000):

$$\frac{\varepsilon_{\mathrm{Si}} - \varepsilon_i}{\varepsilon_i + L_i(\varepsilon_{\mathrm{Si}} - \varepsilon_i)} p_{\mathrm{Si}} + \frac{\varepsilon_{\mathrm{air}} - \varepsilon_i}{\varepsilon_i + L_i(\varepsilon_{\mathrm{Si}} - \varepsilon_i)} (1 - p_{\mathrm{Si}}) = 0 \tag{3}$$

where *i*=xy, z; ε_{Si}, ε_{air} - dielectric permittivities of silicon and air, respectively; p_{Si}– volume fraction of silicon. For a completely oxidized sample, the volume fraction of silicon has to be substituted with that of silica (p_{Silica}).

Two samples of the PSi and $PSiO_2$ layers were fabricated, both on the doped silicon substrate, and characterized by the J. A. Woollam Co. Inc. Variable Angle Spectroscopic Ellipsometer (VASE®). In order to get a large amount of data, the GSE parameters were measured as a function of both angle of incidence and wavelength, in the spectral range from 500 to 1700 nm (the details of data acquisition are described elsewhere (Marino et al, 2007)). All data were simultaneously analysed using WVASE32® software (Woollam et al, 1999) to determine the sample refractive index, thickness, and volume fractions of the constituents.

The samples were initially studied before the LC infiltration in order to find the parameters of the empty porous matrix. After that the E7 liquid crystal was infiltrated and the surface of the porous layers was cleaned from the LC by a flow of pure nitrogen. Temperature of the filled samples was adjusted and stabilized by a processor-controlled hot-stage from CaLCTec S.R.l. which provided temperature stability and accuracy of 0.1 °C.

The empty samples were modelled using the equation (3). The layer thickness, volume fraction of the porous matrix material and depolarization factors were found by fit as follows: h=874±4nm, p_{Si}=15.7±0.1%, L_{xy}=0.356±0.002, and L_z=0.288±0.002 for the PSi sample; and h=423.5±4nm, p_{Silica}=37.0±0.2%, L_{xy}=0.37±0.02, and L_z=0.26±0.02 for the $PSiO_2$ one. The obtained refractive indices n_{xy} and n_z of the anisotropic layers are shown in Fig. 2(a) and 2(b) for PSi and $PSiO_2$ samples, respectively.

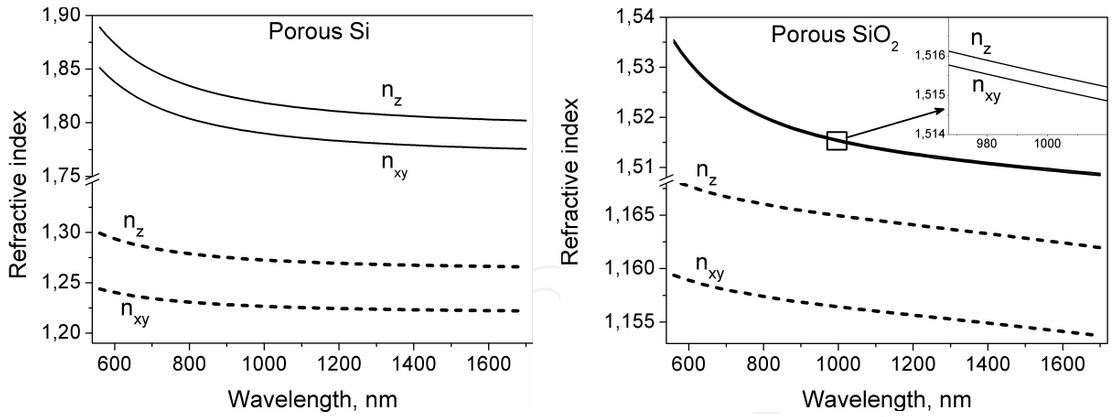

Fig. 2. Refractive indices of PSi (a) and $PSiO_2$ (b) measured for the empty samples (dashed lines) and simulated for the samples filled with E7 at 60°C (solid lines)

One can see that the form birefringence of the PSi matrix is much higher than that of the $PSiO_2$ one (0.05 versus 0.009 at wavelength of 600nm) although the corresponding refractive indices of the samples are quite close. This is explained by much less contrast between refractive index of the pore wall and that of air for the $PSiO_2$ sample as compared with the PSi one.

We have simulated the refractive indices of the porous layers filled with E7 in isotropic phase, using the equation (3) and model parameters for empty samples just substituting the refractive index of void with that of LC (Fig. 2). The dispersion curve of E7 at 60°C was extrapolated from the data of Ref. (Li et al, 2005).

Birefringence of the filled samples decreases to 0.03 and 0.0004 for PSi and $PSiO_2$ samples, respectively. We note that the birefringence of the filled PSi sample is still high while that of the $PSiO_2$ sample can be neglected because of very low refractive index contrast of composite constituents.

Let us remind that the refractive indices of LC have to be found by the fit procedure. Thus the model parameters for the empty porous matrix must be fixed for the filled sample. Otherwise, the strong correlation between the matrix parameters and those of LC gives rise to uncontrollable error in LC refractive indices. Form birefringence of the filled PSi sample is quite high, so the anisotropies of both the porous silicon matrix and the nematic LC contribute to the effective refractive indices of the composite material. As a result, these contributions can not be distinguished and it is impossible to get actual values of refractive indices of the nematic liquid crystal confined in PSi sample.

Since form birefringence of the oxidized sample filled with LC is negligible, we are able to obtain the refractive indices of E7 confined in porous silica. In general LC fills the porous matrix partially (Marino et al, 2007), so we used the Bruggeman formula for three media (Spanier & Herman, 2000): silica, air (in un-filled pores) and LC:

$$\frac{\varepsilon_{\text{Silica}}-\varepsilon_i}{\varepsilon_{\text{Silica}}+2\varepsilon_i}p_{\text{Silica}}+\frac{\varepsilon_{\text{air}}-\varepsilon_i}{\varepsilon_{\text{air}}+2\varepsilon_i}p_{\text{air}}+\frac{\varepsilon_{\text{LC},i}-\varepsilon_i}{\varepsilon_{\text{LC},i}+2\varepsilon_i}p_{\text{LC}}=0\,, \tag{4}$$

where p_{air}, p_{LC} – volume fractions of air and liquid crystal in the medium, respectively; $\varepsilon_{LC,i}$– effective dielectric permittivity of LC inside the pores; other notations are as in (3). Here the LC birefringence is presented by different values $\varepsilon_{LC,xy}$ and $\varepsilon_{LC,z}$.

Using the equation (4) in the optical model we obtained porosity of 62±0.2% which is in a good accordance with the silica volume fraction found above by means of (3). The percentage of LC is 58.4±0.2%, which corresponds to about 94% of pore volume.
The obtained values of E7 indices are shown in Fig. 3 for different temperatures and for two wavelengths.

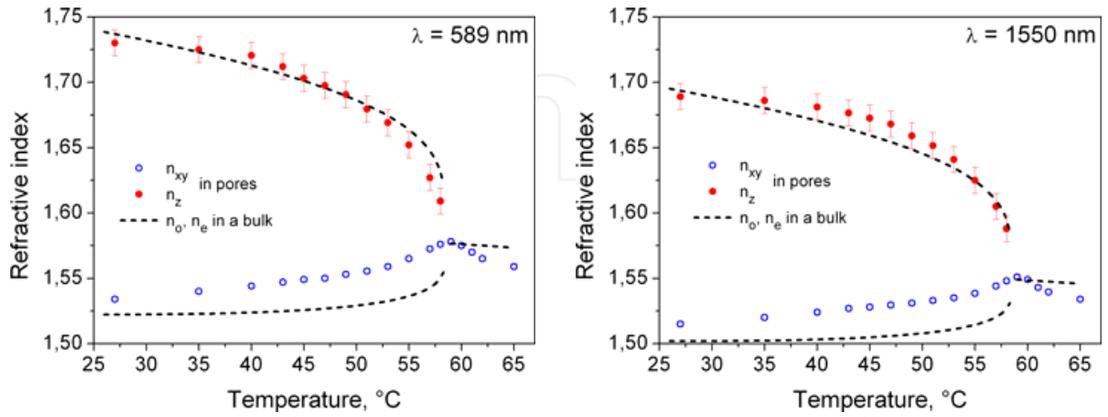

Fig. 3. Refractive index of E7 confined in porous silica (circles) for polarizations parallel (n_{xy}) and perpendicular (n_z) to the sample plane as compared with ordinary (n_o) and extraordinary (n_e) indices of E7 in a bulk (dashed lines) for wavelength of 589nm (a) and 1550nm (b)

For comparison the temperature dependences of the ordinary (n_o) and extraordinary (n_e) indices of E7 in a bulk are presented as extrapolated from the data of Ref. (Li et al, 2005). The clearing point of E7 in pores equals that in a bulk within the error of measurements. Below the clearing point the temperature dependences of n_{xy} and n_z were repeatable while heating or cooling. But if LC becomes isotropic we could not repeat the previous data by cooling and found essential decrease of the refractive index. It is explained by the LC leakage from the pores in isotropic phase.
We have found that n_z of the nematic E7 confined in $PSiO_2$ sample approaches extraordinary refractive index in a bulk, however, the error bars of n_z and n_e measurements are both rather high. The n_{xy} data increase with temperature that means the LC molecules are oriented preferably along the pore axis. At the same time, these data exceed the ordinary refractive index in a bulk. So we conclude that a significant part of the molecules are tilted around the pore axis.

4. Free-standing porous silicon microcavity containing nematic liquid crystal

4.1 Experimental

The design for fabrication represents a quarter-wave microcavity layer with high porosity (etched with current density J = 125 mA/cm²) sandwiched between two 11-period distributed Bragg reflectors (DBR). Alternating high and low (J = 25 mA/cm²) porosity layers form each DBR. We were aimed to obtain the microcavity having resonance within the O-band of telecom optical fibers which utilize wavelengths from 1260 to 1360 nm. Since about 300 nm red shift of the microcavity resonant wavelength is expected after the LC

infiltration (Weiss & Fauchet, 2003), we have designed our structure to have resonance at 1040 nm without LC.

The applied lift-off technique allows the use of the same Si wafer for fabrication of several free-standing structures without disassembling the anodisation container. The first sample, being etched directly from the wafer surface, is always cracked, possibly because of strong mechanical strains. This sample serves as a sacrificial layer leaving the tips of pores on the Si surface after electropolishing (Ouyang et al., 2005). The next sample is free of the thin layer of nanoporous Si on the top and is usually intact. It has open pores which can be easily filled with a liquid crystal. Treatment of the fresh PSi sample with KOH/ethanol solution for 15 minutes scours the pores (Moretti et al., 2006) and slightly improves LC infiltration. The obtained PSi film was placed between two parallel glass plates divided by two spacers (12 μm thick stripes of mylar). After LC infiltration all chinks between the plates were sealed up with an ultraviolet adhesive glue NOA68. Our experimental sample is shown in Fig. 4.

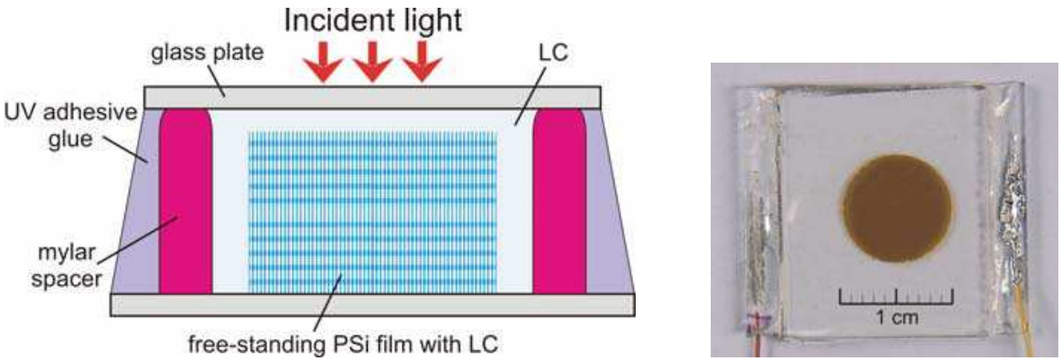

Fig. 4. Microcavity sample: a) scheme, b) top-view picture

Spectral characteristics of the experimental sample were measured using the ellipsometer VASE®. The monochromator of the ellipsometer has the operating waverange from 270 to 1700nm and spectral resolution up to 2 nm. Moreover, we used the fitting facility of the WVASE32® software to specify the parameters of the multilayered PSi structure and to measure the effective refractive index of LC confined in it. During the measurements the PSi-LC filter was contained in a processor-controlled hot-stage, which was mounted on the sample holder of the VASE®.

4.2 Simulation of optical properties of a PSi film with LC

To calculate spectra of a multilayer PSi structure one has to define the refractive indices and thicknesses of all layers. When the sample is not filled with LC, the Bruggeman formula (4) for two media, namely silicon and air, is applied. Infiltration with LC complicates simulation of the layer refractive index. First of all, the effective refractive index n_{LC} of liquid crystal in pores depends on the spatial distribution of the local director **L**. In the nematic phase, the LC director field depends on the interplay between molecular surface anchoring, elastic energies of the liquid crystal, and forces caused by external fields, if any. Here the director field of the nematic mixture E7 confined in cylindrical pores is calculated using the Frank's free energy approach (Crawford et al, 1992; Tkachenko et al, 2008). If there is no external influence, the free energy F of the confined nematic is given by (Crawford et al, 1992):

$$F = \frac{1}{2}\int_{\text{vol}} \{ \mathrm{K}_{11} \cdot \left(\text{div}(\mathbf{L})\right)^2 + \mathrm{K}_{22} \cdot \left(\mathbf{L} \cdot \text{curl}(\mathbf{L})\right)^2 + \mathrm{K}_{33} \cdot \left(\mathbf{L} \times \text{curl}(\mathbf{L})\right)^2 - \mathrm{K}_{24} \cdot \text{div}\left(\mathbf{L} \times \text{curl}(\mathbf{L}) + \mathbf{L} \cdot \text{div}(\mathbf{L})\right) \} \, dV + \frac{1}{2}\int_{\text{surf}} \left(W \cdot \sin^2 \Omega\right) dS, \quad (5)$$

where K_{11}, K_{22} and K_{33} are the specific elastic constants for the bulk deformations: splay, twist and bend, respectively; K_{24} is the saddle-splay surface elastic constant; $\mathbf{L} = \cos(\Omega(r)) \cdot \mathbf{z} + \sin(\Omega(r)) \cdot \mathbf{r}$ is the nematic director, which represents the local direction of the LC optical axis; W is the molecular anchoring strength; Ω is the angle between **L** and the pore axis.

For cylindrical cavities there are five stable non-twisted configurations of the nematic director field depending on the anchoring conditions: uniform axial (UA), planar radial, planar polar, escaped radial (ER) and escaped radial with point defects. According to (Leonard et al., 2000; Haurylau et al., 2006) E7 exhibits ER configuration in the pores larger than 1 μm in diameter. This configuration occurs when LC molecules are anchored homeotropically, i.e. perpendicular to the pore walls, and the director **L** escapes into the third dimension toward the axis of the pore. While for the UA configuration the local director is oriented parallel to the pore axis in the whole volume. In our case of the mesoporous silicon there is a lack of information on the LC director field configuration, however the ellipsoid of the effective refractive index of LC is found to be uniaxial with its long axes oriented normally to the plane of a PSi layer (Marino et al, 2007). This can be explained by ER or UA configurations of LC director. We assume the ER configuration for our samples because it matches better the experimental spectra as will be shown in Section 4.3. So the molecular system in a pore has axial symmetry and the equation (5) depends only on the radial coordinate r.

To simulate the LC director field Ω(r), we used a well-known method of minimization of the free energy (Crawford et al, 1992). In the case of ER configuration, the expression (5) can be set in the form:

$$F = \pi h \, \mathrm{K}_{11} \int_0^{\mathrm{R}} F_0 \, dr + \pi R W \, , \quad (6)$$

$$F_0 = \frac{\sin^2 \Omega}{r} + r \cdot (\Omega')^2 \left(\cos^2 \Omega + k \cdot \sin^2 \Omega\right) - 2\sigma\Omega' \sin\Omega\cos\Omega \, , \quad (7)$$

where Ω' is the first derivative of Ω(r); k = K_{33}/K_{11}; R is the pore radius; $\sigma = RW/\mathrm{K}_{11} + \mathrm{K}_{24}/\mathrm{K}_{11} - 1$ is a dimensionless surface parameter. Minimization of the free energy F_0 gives the second order differential equation:

$$\Omega''\left(\cos^2 \Omega + k \sin^2 \Omega\right) + (\Omega')^2 \sin\Omega \cos\Omega \, (k-1) + \frac{\Omega'}{r}\left(\cos^2 \Omega + k \sin^2 \Omega\right) - \frac{1}{r^2}\sin\Omega\cos\Omega = 0 \, , \quad (8)$$

which can be solved numerically using the following boundary conditions:

$$\Omega\big|_{r=0} = 0; \quad \Omega'\big|_{r=R} = \frac{\sigma \sin\Omega_R \cos\Omega_R}{R \cdot \left(\cos^2\Omega_R + k \cdot \sin^2\Omega_R\right)}, \quad \text{where } \Omega_R = \Omega\big|_{r=R}. \tag{9}$$

When the director field Ω(*r*) of LC inside the silicon pore is found, the effective dielectric permittivity and refractive index of the nematic LC in a cylindrical pore is calculated by the formula (Tkachenko et al, 2008):

$$\varepsilon_{LC} = n_{LC}^2 = \frac{1}{R^2}\int_0^R \left[2\varepsilon_o + \left(\varepsilon_e - \varepsilon_o\right)\sin^2\Omega(r)\right] r\,dr, \tag{10}$$

where ε_o, ε_e – ordinary and extraordinary components of the LC dielectric permittivity at near infrared range.

The effective dielectric permittivity of each layer of the PSi film for in-plane polarization (*i*=xy) is calculated by means of the equation (4) replacing "Silica" by "Si" in the subscripts. We assume percentage of the pore volume filled by LC (p'_{LC}) to be independent on porosity. This value is defined as:

$$p'_{LC} = p_{LC}/\left(1 - p_{Si}\right). \tag{11}$$

The LC volume fraction in PSi can not be measured directly. So we determine it by fit of the simulated spectra of the microcavity to the experimental data when the sample is heated over the clearing point of the LC. For the fit, the p'_{LC} value is the only variable parameter. Finally, the well-known transfer matrix method (TMM) (Born & Wolf, 1980) is applied to calculate the theoretical spectra of the PSi-LC multilayer structure.

4.3 Results and discussion

The experimental transmittance spectrum of the empty free-standing PSi microcavity is shown by solid dots in Fig. 5(a). The spectrum has the central stop-band in the wave range of 950-1150 nm with several side lobes and the second harmonic band-gap centered at 540 nm which are the features of the Bragg reflectors. A sharp resonant peak is observed at the wavelength of 1038 nm inside the central stop-band due to the presence of the microcavity layer. Light absorption by silicon causes a steep decrease of the transmittance in the visible.

We used the WVASE32® software to analyze this spectrum. The optical model contained all the layers of the filter described above including the glass substrates. The PSi film was described as a periodic lattice of EMA layers. The parameters of the PSi layers were obtained by the fit procedure matching the data generated by the model with the experimental ones (Fig. 5(a)). The fit gave void fraction of 79.8% and 72.3% for the layers with high and low porosity, respectively.

The spectra of the structure filled with E7 are presented in Fig. 5(b) for temperature values of 27°C and 65°C. The lower temperature value corresponds to the nematic phase while the higher one corresponds to the deep (8 degree higher than the clearing point) isotropic phase of the E7 liquid crystal. As may be seen, the microcavity peak is red-shifted by more than 300 nm as compared with the empty structure. This shift comes from the increase of the effective refractive indices of PSi layers. After LC infiltration the microcavity Q-factor falls to 37 from the value of 58 exhibited in the case of the empty filter, since the refractive index contrast decreases and the Bragg condition is not held for all the layers at the same wavelength.

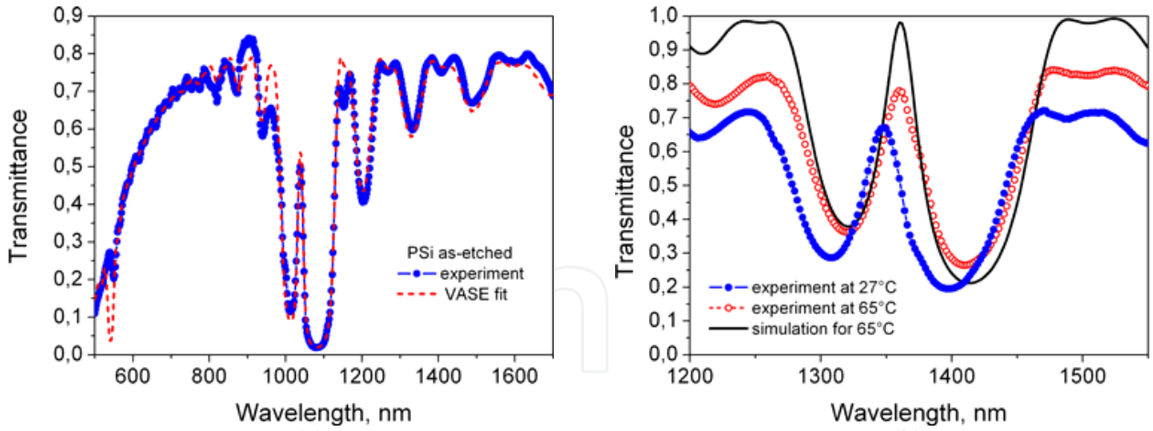

Fig. 5. a) Transmittance spectra of the empty PSi microcavity: experimental (solid dots) and fitted by WVASE32® (dashed line). b) Spectra of the sample filled with E7: measured at 65°C (solid dots) and 27°C (circles) and calculated for 65°C (solid line)

Optical properties of the free-standing film with LC were simulated using the numerical method developed as described above. The main advantage of this method, as compared with WVASE32®, is the ability to simulate orientational properties of LC.

In Fig. 5(b) the solid line shows the simulated spectrum which can be considered in a good accordance with the experimental curve if one takes into account the simplifications of the model used for calculations. Our model neglects energy losses due to reflection at the first interface, absorption in silicon, losses in the LC layer above the PSi film, and scattering at the interfaces of the multilayer structure. That is why the maximum transmittance of the experimental curve is about 20% lower than the calculated one. What is important for our study, the simulated position of the resonance peak and the stop-band shape match the experimental data.

We note that the finite size glass substrates (with thickness of 1 mm) should give rise to a great number of very sharp peaks in the simulated spectra of the multilayer PSi structure. These peaks correspond to the modes of the glass layers and appear at the spectral curves with a period of 0.3 nm and amplitude up to 0.3 in transmittance. However, these peaks were not resolved in experiments due to the low spectral resolution of the used monochromator. To avoid the presence of these un-necessary peaks in the simulations, the glass substrates were considered infinite.

In the simulation, we used the dispersion curve of the n_{LC} for E7 in the isotropic state, derived from literature (Li et al, 2005). The best fit of the simulated spectrum to the experimental one corresponds to $p'_{LC} = 0.843$. The fraction of the LC in the composite is equal to 67.3% and 60.9% for the high and low porosity layers, respectively.

Heating the sample gives rise to a red shift of the spectrum (Fig. 5(b)), due to the increase with temperature of the effective refractive index of the LC confined in the pores. The detailed temperature dependence of the resonance wavelength shift is plotted in Fig. 6(a). This thermal tuning is due to the temperature dependence of n_{LC}. It is nonlinear in the nematic phase with the highest slope near the clearing point of E7. The red shift of the resonance wavelength proves that possible director configuration is either UA or ER. Above the clearing point the resonance position is almost independent of temperature. For our sample, thermal tuning of the resonance wavelength was entirely reversible within the range of 13 nm.

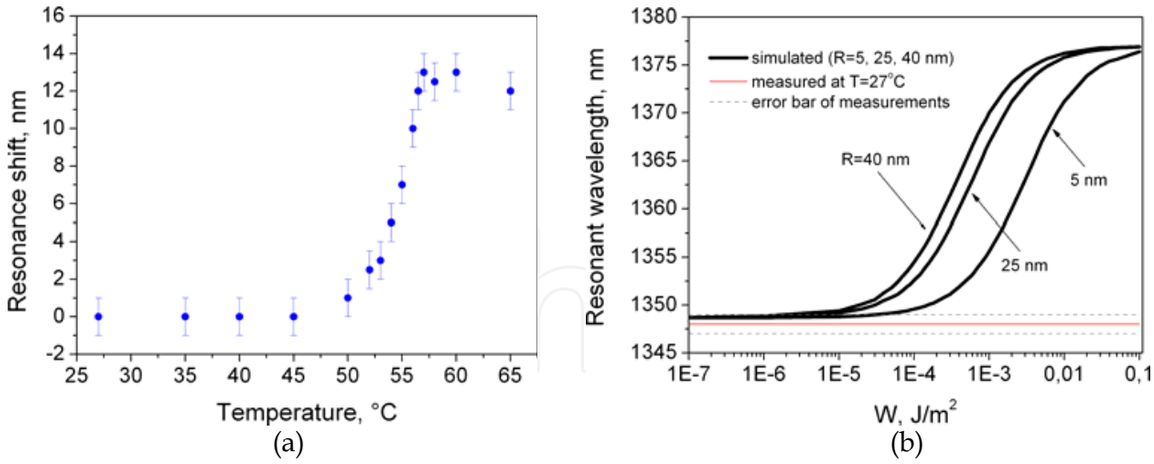

Fig. 6. a) Temperature dependence of the microcavity resonance shift. b) Resonant wavelength of the microcavity versus the surface anchoring strength W

The tuning range is defined by the difference between the n_{LC} values at the room temperature and at the clearing point. The latter value is well known (Li et al., 2005), while to predict the former one we have to simulate the effective refractive index of E7 taking into account the nematic director configuration inside the pores. Comparing the spectra simulated for the different director fields with the experimental one helps to define the actual LC director configuration in the investigated PSi film.

The director field in the ER configuration was calculated using the Frank's free energy approach. We have used the following constants for E7 (Crawford et al, 1992; Leonard et al., 2000; Tkachenko et al, 2008]: K_{11} = 11.1 pN; K_{33} = 17.1 pN; K_{24} = 28.6 pN and the dispersion curves for ordinary and extraordinary indices from (Abbate et al., 2007). According to (Crawford et al, 1992; Leonard et al., 2000), the surface anchoring strength W for the E7 in supramicrometer silicon pores is estimated to be 10^{-5} J/m^2. Because the magnitude of W in mesopores is unknown, we took it variable in our computations. The dependence of the microcavity resonance wavelength on the molecular anchoring strength is shown in Fig. 6(b). The curves computed for different values of the pore radius are shown by the thick solid lines. The value of 25 nm is the averaged pore radius, while the values of 5 and 40 nm are the minimum and maximum pore radii occurred in our experimental PSi films. Experimental position of the resonance peak at 27°C and the error bar of the measurements are presented by the horizontal thin solid and dashed lines, respectively. As may be seen from the figure, the simulated curves approach the experimental resonant wavelength for W<10^{-6} J/m^2. Moreover, in this case the calculated resonance position does not depend on the pore radius. Thus, we take W = 10^{-6} J/m^2 and R=25 nm in simulations of $\Omega(r)$ for the ER director configuration.

Finally, we have performed the simulations of the spectra using the n_{LC} value given by equation (10) for the ER configuration and $n_{LC} = n_o$ for the UA configuration. The LC fraction inside the pore volume was taken equal to 84.3% as found above. The calculated spectra both for the ER and UA cases are shown in Fig. 7(a) together with the spectrum measured at 27°C.

As may be seen, the ER-curve is much more similar to the experimental spectrum (the values of the resonance wavelength match very well). Consequently, the actual LC configuration in silicon mesopores is not UA but it is close to ER.

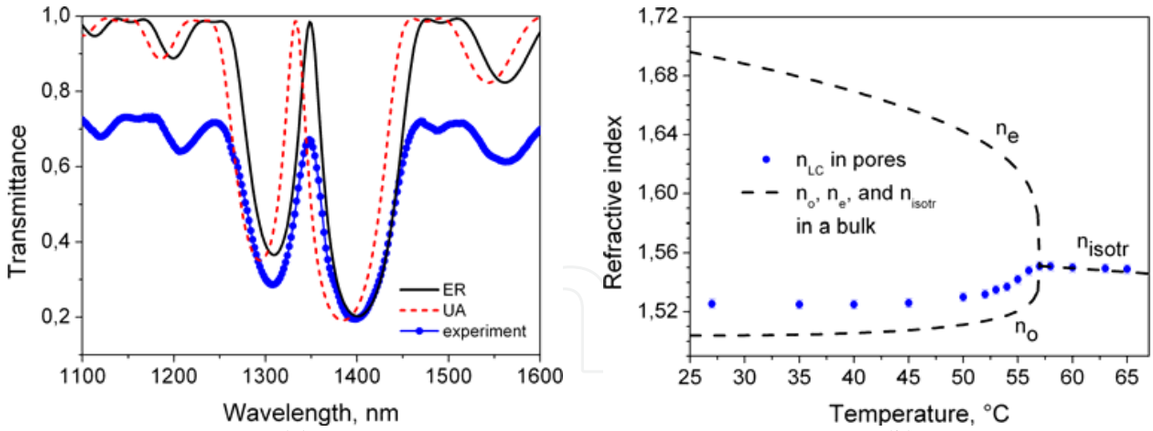

Fig. 7. a) Calculated spectra of the PSi-LC structure for ER (solid line) and UA (dashed line) director configurations of the LC. Experimental spectrum (solid dots) at 27°C is given for comparison. b) Effective refractive index of E7 in pores fitted by WVASE32® (solid dots) and values of n_o, n_e and n_{isotr} in a bulk (Li et al., 2005) (dashed lines)

Simulation of the spectra by the WVASE32® confirms this statement. Unlike the abovementioned numerical method, WVASE32® does not compute the effective refractive index of the LC in the pores but finds it from the fit of the generated and experimental spectra. The optical model of the structure implied the layer thicknesses, porosity values and the fraction of the LC as specified above, while two parameters of the Cauchy formula for the LC refractive index were varied during the fit procedure. Fig. 7(b) shows the temperature dependence of n_{LC} at 1300 nm in comparison with the refractive indices of E7 in the bulk (Li et al., 2005) in the nematic (n_o, n_e) and isotropic (n_{isotr}) phases. For the UA configuration of the LC director n_{LC} would be equal to n_o (at normal incidence of the light). As it is evident from Fig. 7(b), in our case n_{LC} is significantly larger than n_o. This fact is in accordance with the results obtained for E7 confined in the porous silica monolayer (see Section 3).

5. Electrical reorientation of LC molecules inside cylindrical pore: theoretical approach

Fig. 8 shows the model of a cylindrical pore filled with a liquid crystal under the influence of an electric field. In the ER configuration the LC director field has axial symmetry, so it is described by only one parameter, namely the angle Ω between LC director and the pore axis. At the pore edges, transparent electrodes are connected to a voltage supply to produce the electric field.

The director field configuration of the LC inside a pore depends on its elastic properties, the strength and preferred orientation of molecular surface anchoring, and the electrostatic forces caused by the applied electric field. The free energy of a confined nematic is given by (Crawford et al., 1992):

$$\widetilde{F} = F - \frac{1}{2}\int_{\mathrm{vol}} (\mathbf{D}\cdot\mathbf{E})\mathrm{d}V. \tag{12}$$

where **E**, **D** are the electric field strength and displacement vectors, respectively. In the case of ER configuration, the expression (5) can be set in the form:

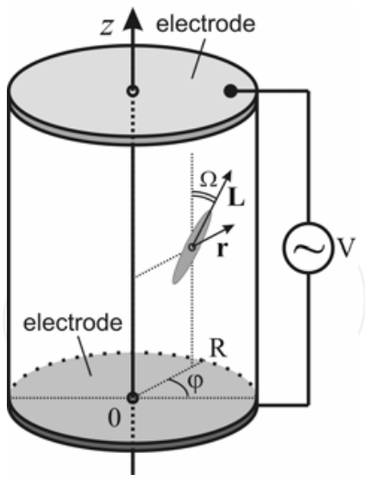

Fig. 8. Liquid crystal molecule inside a cylindrical pore

$$\widetilde{F} = \pi h \, \mathrm{K}_{11} \int_0^{\mathrm{R}} \left(F_0 - \frac{r \, \varepsilon_{\mathrm{v}} \varepsilon_{\perp} \varepsilon_{\parallel}}{\mathrm{K}_{11}(\varepsilon_{\perp} + \Delta\varepsilon \sin^2 \Omega)} E^2 \right) \mathrm{d}r + \pi R W \, , \tag{13}$$

where ε_v is the permittivity of vacuum; $\varepsilon_{\perp}$, $\varepsilon_{\parallel}$ are the components of the LC permittivity normal and parallel to **L**; $\Delta\varepsilon = \varepsilon_{\parallel} - \varepsilon_{\perp}$; E – the electric field component parallel to the pore axis. It is important to distinguish $\varepsilon_{\perp}$, $\varepsilon_{\parallel}$, low frequency permittivities, from ε_o and ε_e. Minimization of $\widetilde{F}$ gives the second order differential equation:

$$\begin{aligned} &\Omega''\left(\cos^2 \Omega + k \sin^2 \Omega\right) + \left(\Omega'\right)^2 \sin\Omega \cos\Omega \, (k-1) + \frac{\Omega'}{r}\left(\cos^2 \Omega + k \sin^2 \Omega\right) \\ &- \frac{1}{r^2} \sin\Omega \cos\Omega - \frac{\varepsilon_{\mathrm{V}} \, \varepsilon_{\perp} \, \varepsilon_{\parallel} \, E^2 \Delta\varepsilon \sin\Omega \cos\Omega}{\mathrm{K}_{11} \left(\varepsilon_{\perp} + \Delta\varepsilon \sin^2 \Omega\right)^2} = 0 \, . \end{aligned} \tag{14}$$

The equation (14) is solved numerically using the boundary conditions (9), where Ω_R is a function of E.

For simulation of nematic E7 director field within a cylindrical pore we used the following constants: R = 10, 25, 75, and 150 nm; W = 10^{-6}, 10^{-5}, $5{\cdot}10^{-5}$, 10^{-4}, and $5{\cdot}10^{-4}$ J/m^2; $\varepsilon_{\parallel}$ = 19.0; $\varepsilon_{\perp}$ = 5.2 (Crawford et al., 1992; Leonard et al., 2000). The simulated director field for different values of the electric field E at W = 10^{-5} J/m^2 and R=75 nm is shown in Fig. 9.

The director is axially aligned at the pore axis (r = 0) and rotates as a function of radius to a certain angle Ω_R at the pore wall (r = R). In the case of zero electric field the director distribution agrees with that simulated in (Leonard et al., 2000). The LC molecules reorient toward the pore axis direction with E increasing. Above the critical field value E_{UA} which is about 3.8 V/μm for the used pore parameters, the LC molecular configuration becomes uniform axial.

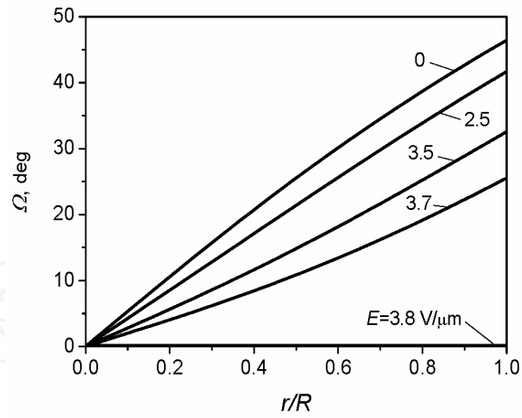

Fig. 9. Nematic director distribution in a pore for E=0, 2.5, 3.5, 3.7, and 3.8 V/μm; R =75 nm

The calculated n_{LC} versus E at different surface anchoring strength W are shown in Fig. 10(a). While electric field increases, the effective index tends to the minimum value of 1.501, which corresponds to the case of the uniform axial configuration. Furthermore, the higher is the surface anchoring strength W, the wider the range of refractive index tuning and higher the corresponding E_{UA} value.

The value of n_{LC} versus the applied electric field at different pore radius R is shown in Fig. 10(b). Reduction of the average pore radius causes insignificant decrease of the tuning range of refractive index. At the same time, E_{UA} value promptly grows. Therefore, the use of PSi with wider pores is required for devices operating at lower voltages. Because multilayer microcavities usually have an overall thickness of about 10 micron, a pore radius above 75 nm has to be chosen for the applied voltage to be less than 40 V, in the case of weak anchoring (W=10^{-5} J·m^{-2}). For stronger anchoring, the pores should be larger. However, it is noteworth remembering that excessive increase of the pore size is restricted by the growth of light scattering and violation of the Bruggeman approximation. On the other hand, these restrictions do not hold anymore when the pores are distributed periodically, as in 2-D photonic crystals. Hence, strong anchoring conditions can be used to increase Ω_R and the tuning range of such devices.

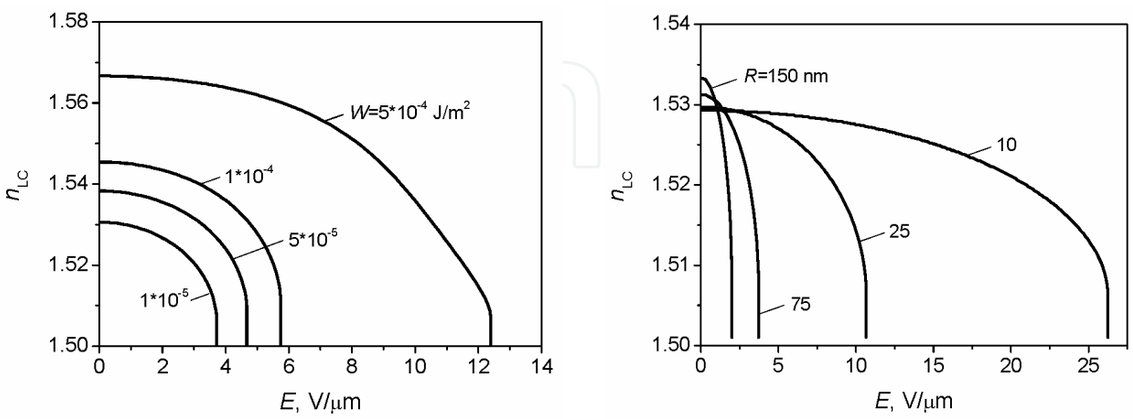

Fig. 10. Effective refractive index of the pore volume filled with E7 versus electric field: a) for W = 10^{-5}, 5·10^{-5}, 10^{-4}, 5·10^{-4} J/m^2; R=75 nm; b) for R = 10, 25, 75, 150 nm; W=10^{-5} J/m^2

While electric field is applied to a multilayer PSi filled with the liquid crystal the value of n_{LC} goes down causing the decrease of the effective refractive index of each porous layer. As an example, we simulated spectra of the multilayer structure containing a microcavity sandwiched between two PSi distributed Bragg reflectors with alternating layers of 50% and 80% porosity, filled with E7 and tuned by the external electric field (Tkachenko et al., 2008). Shift of the microcavity resonance versus electric field is shown in Fig. 11.

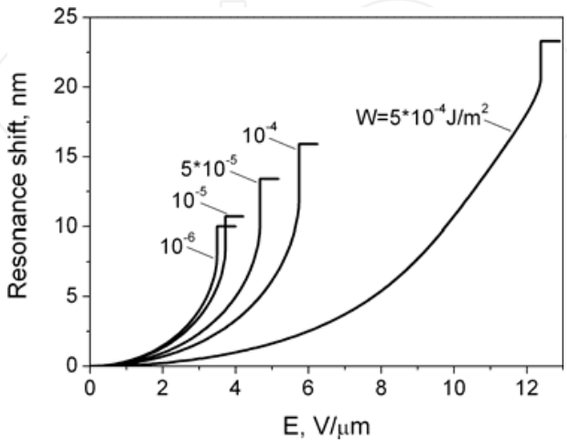

Fig. 11. Blue shift of the resonance versus electric field for $W = 10^{-6} \div 5 \cdot 10^{-4}$ J/m^2; R=75 nm

As may be seen, the electrical tuning range of the microcavity resonance varies from 10 nm up to 23 nm for weak and strong surface anchoring conditions, respectively. The electric field required for the maximum shift in the case of weak anchoring is about 3.5 V/μm, while for the strong anchoring it rises to 12.4 V/μm.

6. Conclusion

We have investigated properties of the nematic liquid crystal mixture E7 confined in thin porous films fabricated by electrochemical etch of silicon wafers. The use of spectroscopic ellipsometry is proposed for deriving information about volume fraction, effective ordinary and extraordinary refractive indices and preferred director orientation of the confined nematic.

An empty porous silicon film has rather high birefringence and after infiltration with the isotropic liquid crystal the birefringence of the resultant composite is still significant. Anisotropy of the porous silicon matrix hinders the measurements of the refractive indices of the nematic liquid crystal confined in pores. However, ellipsometry was successful in characterizing E7, in the completely oxidized sample. Relatively small form birefringence of porous silica decreases by a factor of 20 when E7 is infiltrated into the pores, because of the low refractive index contrast between the liquid crystal and silica. Thus, we considered the porous host as isotropic and derived the refractive indices of the anisotropic liquid-crystalline guest.

The free-standing mesoporous silicon microcavity infiltrated with E7 was designed and studied. Transmission spectra of the device were measured at different temperatures using the spectroscopic ellipsometer. Heating the nematic in pores results in the continuous red shift of the peak in the range of 13 nm. The Frank's free energy approach with assumption of escape radial configuration was applied for simulation of orientational properties of the

nematic confined in silicon mesopores. The proposed method allows reliable calculation of the range of thermal tuning of interference filters based on porous silicon with liquid crystals.

We have simulated the reorientation of the local director of a nematic liquid crystal confined inside a silicon pore under external electric field influence. On the base of this simulation the maximum tuning range for porous silicon microcavity infiltrated with E7 was obtained for different values of the surface anchoring strength and pore radius. It was found that for strong anchoring a wider range of electrical tuning can be obtained than for weak anchoring, but a higher electric field is required.

Basically, devices with thermal tuning are much slower than electrically tuned ones. In this connection, an alternative and attractive idea would be to produce a local heating of liquid crystals in porous silicon by laser beam illumination, for the realization of a fast all-optical modulator, which is the subject of our future work.

7. Acknowledgements

The authors would like to thank Lucia Rotiroti, Edoardo De Tommasi and Principia Dardano from Istituto per la Microelettronica e Microsistemi (CNR-IMM, Naples, Italy) for their help with fabrication of samples, and Ivo Rendina, head of the Institute, for helpful discussion and financial support.

8. References

Abbate, G.; Tkachenko, V.; Marino, A.; Vita, F.; Giocondo, M.; Mazzulla, A. & De Stefano, L. (2007). Optical characterization of liquid crystals by combined ellipsometry and half-leaky-guided-mode spectroscopy in the visible-near infrared range. *Journal of Applied Physics.* Vol. 101, No. 7, April 2007, 073105-073105-9, ISSN: 0021-8979

Born, M. & Wolf, E. (1980). *Principle of Optics,* 6th edn., Pergamon Press, ISBN: 0080264816, Oxford

Canham, L. (1990). Silicon quantum wire array fabrication by electrochemical and chemical dissolution of wafers. *Applied Physics Letters.* Vol. 57, No. 10, September 1990, 1046-1048, ISSN: 0003-6951

Canham, L. (1997). *Properties of Porous Silicon*, Inspec/IEE, ISBN: 0852969325, London

Crawford, G.; Allender, D. & Doane, J. (1992). Surface elastic and molecular-anchoring properties of nematic liquid crystals confined to cylindrical cavities. *Physical Review A*, Vol. 45, No. 12, June 1992, 8693-8708, ISSN: 1050-2947

Crawford, G. & Žumer, S. (1996). *Liquid Crystals in Complex Geometries*, Taylor & Francis Ltd, ISBN: 0-7484-0464-3

De Stefano, L.; Rea, I.; Rendina, I.; Rotiroti, L.; Rossi, M. & D'Auria, S. (2006). Resonant cavity enhanced optical microsensor for molecular interactions based on porous silicon. *Physica Status Solidi A.* Vol. 203, No. 5, 886-891, ISSN: 0031-8965

Ghulinyan, M.; Oton, C.; Bonetti, G.; Gaburro, Z. & Pavesi, L. (2003). Free-standing porous silicon single and multiple optical cavities. *Journal of Applied Physics.* Vol. 93, No. 12, June 2003, 9724-9729, ISSN: 0021-8979

Haurylau, M.; Anderson, S.; Marshall, K. & Fauchet, P. (2006). Electrical modulation of silicon-based two-dimensional photonic bandgap structures. *Applied Physics Letters,* Vol. 88, February 2006, 061103-1 - 061103-3, ISSN: 0003-6951

Lehmann, O. (1904). *Flüssige Kristalle*, W. Engelmann, Leipzig

Lehmann, V & Gösele, U. (1991). Porous silicon formation: a quantum wire effect, *Applied Physics Letters.* Vol. 58, No. 8, February 1991, 856, ISSN: 0003-6951

Leonard, S.; Mondia, J.; van Driel, H.; Toader, O.; John, S.; Busch, K.; Bimer, A.; Gosele, U. & Lehmann, V. (2000). Tunable two-dimensional photonic crystals using liquid-crystal infiltration. *Physical Review B*, Vol. 61, No. 4, January 2000, R2389 - R2392, ISSN: 0163-1829

Leonard, S.; van Driel, H.; Busch, K; John, S.; Birner, A.; Li, A.; Muller, F.; Gosele, U. & Lehmann, V. (1999). Attenuation of optical transmission within the band gap of thin two-dimensional macroporous silicon photonic crystals. *Applied Physics Letters.* Vol. 75, No. 20, November 1999, 3063-3065, ISSN: 0003-6951

Li, J.; Wu, S.; Brugioni, S.; Meticci, R. & Faetti, S. (2005). Infrared refractive indices of liquid crystals. *Journal of Applied Physics.* Vol. 97, No. 7, March 2005, 073501-1 – 073501-5, ISSN: 0021-8979

Marino, A.; Abbate, G.; Tkachenko, V.; Rea, I.; De Stefano, L. & Giocondo, M. (2007). Ellipsometric study of liquid crystal infiltrated porous silicon. *Molecular Crystals and Liquid Crystals.* Vol. 465, April 2007, 359-370, ISSN: 1542-1406

Moretti, L.; Rea, I.; Rotiroti, L.; Rendina, I.; Abbate, G.; Marino, A. & De Stefano, L. (2006). Photonic band gaps analysis of Thue-Morse multilayers made of porous silicon. *Optics Express,* Vol. 14, No. 13, June 2006, 6264 – 6272, ISSN: 1094-4087

Ouyang, H.; Christophersen, M.; Viard, R.; Miller, B. & Fauchet, P. (2005). Macroporous Silicon Microcavities for Macromolecule Detection *Advanced Functional Materials*. Vol. 15, No. 11, 1851-1859, ISSN: 1616-301X

Pap, A.; Kordás, K.; Tóth, G.; Levoska, J.; Uusimäki A.; Vähäkangas, J.; Leppävuori, S. & George, T. (2005). Thermal oxidation of porous silicon: study on structure. *Applied Physics Letters.* Vol. 86, No. 4, January 2005, 041501-1 – 041501-3, ISSN: 0003-6951

Pavesi, L. & Dubos, P. (1997). Random porous silicon multilayers: application to distributed Bragg reflectors and interferential Fabry-Perot filters. *Semiconductor Science and Technology*. Vol. 12, No. 5, May 1997, 570-575, ISSN: 0268-1242

Pirasteh, P.; Charrier, J.; Soltani, A.; Haesaert, S.; Haji, L.; Godon, C. & Errien, N. (2006). The effect of oxidation on physical properties of porous silicon layers for optical applications *Applied Surface Science*. Vol. 253, No. 4, December 2006, 1999–2002, ISSN: 0169-4332

Spanier, J. & Herman, I. (2000). Use of hybrid phenomenological and statistical effective-medium theories of dielectric functions to model the infrared reflectance of porous SiC films. *Physical Review B*. Vol. 61, No. 15, April 2000, 10437-10450, ISSN: 1098-0121

Tkachenko, V.; Dyomin, A.; Tkachenko, G.; Abbate, G. & Sukhoivanov, I. (2008). Electrical reorientation of liquid crystal molecules inside cylindrical pores for photonic device applications. *Journal of Optics A: Pure and Applied Optics.* Vol. 10, No. 5, May 2008, 055301-1 – 055301-6, ISSN: 1464-4258

Turner, D. (1958). Electropolishing silicon in hydrofluoric acid solutions. *Journal of the Electrochemical Society*. Vol. 105, No. 7, July 1958, 402-408, ISSN: 0013-4651

Uhlir, A. (1956). Electrolytic shaping of germanium and silicon. *The Bell System Technical Journal*. Vol. 35, March 1956, 333-347, ISSN: 1089-7089

Weiss, S. & Fauchet, P. (2003). Electrically tunable porous silicon active mirrors. *Physica Status Solidi A*. Vol. 197, No. 2, May 2003, 556-560, ISSN: 0031-8965

Weiss, S.; Ouyang, H.; Zhang, J. & Fauchet, P. (2005). Electrical and thermal modulation of silicon photonic bandgap microcavities containing liquid crystals. *Optics Express*. Vol. 13, No. 4, February 2005, 1090-1097, ISSN: 1094-4087

Woollam, J.; Johs, B; Herzinger, C.; Hilfiker, J.; Synowicki, R. & Bungay, C (1999). Overview of Variable Angle Spectroscopic Ellipsometry (VASE), Part I: Basic Theory and Typical Applications, Proceedings of Optical Metrology, CR72, pp. 3-28, ISBN: 0819432350, Denver, Colorado, July 1999, SPIE, Bellingham, Washington

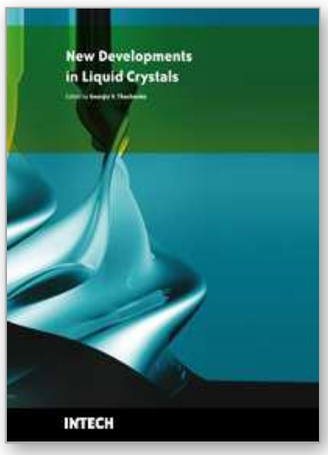

New Developments in Liquid Crystals

Edited by Georgiy V Tkachenko

ISBN 978-953-307-015-5
Hard cover, 234 pages
Publisher InTech
Published online 01, November, 2009
Published in print edition November, 2009

Liquid crystal technology is a subject of many advanced areas of science and engineering. It is commonly associated with liquid crystal displays applied in calculators, watches, mobile phones, digital cameras, monitors etc. But nowadays liquid crystals find more and more use in photonics, telecommunications, medicine and other fields. The goal of this book is to show the increasing importance of liquid crystals in industrial and scientific applications and inspire future research and engineering ideas in students, young researchers and practitioners.

How to reference

In order to correctly reference this scholarly work, feel free to copy and paste the following:

Georgiy V. Tkachenko, Volodymyr Tkachenko, Giancarlo Abbate, Luca De Stefano, Ilaria Rea and Igor A. Sukhoivanov (2009). Nematic Liquid Crystal Confined in Electrochemically Etched Porous Silicon: Optical Characterization and Applications in Photonics, New Developments in Liquid Crystals, Georgiy V Tkachenko (Ed.), ISBN: 978-953-307-015-5, InTech, Available from: http://www.intechopen.com/books/new-developments-in-liquid-crystals/nematic-liquid-crystal-confined-in-electrochemically-etched-porous-silicon-optical-characterization-

INTECH
open science | open minds

InTech Europe
University Campus STeP Ri
Slavka Krautzeka 83/A
51000 Rijeka, Croatia
Phone: +385 (51) 770 447
Fax: +385 (51) 686 166
www.intechopen.com

InTech China
Unit 405, Office Block, Hotel Equatorial Shanghai
No.65, Yan An Road (West), Shanghai, 200040, China
中国上海市延安西路65号上海国际贵都大饭店办公楼405单元
Phone: +86-21-62489820
Fax: +86-21-62489821

IntechOpen